Supplementary part of "Mechanisms of plasma disruption and runaway electron losses in the TEXTOR tokamak"

S. S. Abdullaev[1] †, K.H. Finken[2], K. Wongrach[2], M. Tokar[1], H.R. Koslowski[1], O. Willi[2], L. Zeng[3], and the TEXTOR team

[1] Forschungszentrum Jülich GmbH, Institut für Energie- und Klimaforschung - Plasmaphysik, D–52425 Jülich, Germany.
[2] Institut für Laser- und Plasmaphysik, Heinrich-Heine Universität Düsseldorf, Germany
[3] Institute of Plasma Physics, Chinese Academy of Sciences, 230031 Hefei, China

(Received ?; revised ?; accepted ?. - To be entered by editorial office)

In Supplementary part we present theoretical techniques employed to study mechanisms of plasma disruption and the formation of runaway electrons in tokamaks. First, the relativistic Hamiltonian equations for guiding–center motion in a toroidal system are recalled. The models for magnetic fields of the pre–disruption equilibrium plasma and a stochastic magnetic field during a plasma disruption are described. The effects of a toroidal electric field and magnetic perturbations on the dynamics of electrons are analyzed. Particularly, the formula for the outward drift velocity in a toroidal electric field is derived. To study heat and particle transport during thermal and current quench regimes we used the model of a stochastic magnetic field. The test particle transport model is used to estimate thermal and current quench times. magnetic field

1. Introduction

Supplementary part of the paper consists of six sections. In Sec. 2 the Hamiltonian equations of relativistic guiding–center (GC) motion is a toroidal system are recalled. The descriptions of the models for pre–disruption equilibrium plasma, the toroidal electric field, the MHD modes, and the dynamic ergodic divertor (DED) of the TEXTOR tokamak are given in Secs. 3, 4, 5.1, and 5.2, respectively. The particle dynamics in the presence of magnetic perturbations is studied in Secs. 6.1, 6.2, and 6.3. Hamiltonian equations for the magnetic field lines and the model of a stochastic magnetic field used to simulate the heat and particle transport is described in Secs. 7.1 and 7.2. In Sec. 7.4 the collisional transport model in a stochastic magnetic field is recalled and it is used to calculate the radial diffusion coefficients of electrons and particles during the fast phase and the current decay phase of plasma disruption.

2. Guiding–center motions in toroidal plasmas

To study the RE orbits we employ the version of the relativistic Hamiltonian equations for a GC motion in a toroidal system given in Refs. (Abdullaev & Finken 2002; Abdullaev *et al.* 2006; Wingen *et al.* 2006) (see Chapt. 4 in (Abdullaev 2014) for more details). In this section the brief description of the corresponding equations is given.

We use the cylindrical coordinate system (R, Z, φ), where R, Z are the radial and vertical coordinates, respectively, and φ is the toroidal angle. For generality, we consider

† Email address for correspondence: s.abdullaev@fz-juelich.de

a motion of a charged particle of mass m_0 and a charge $q_a = Z_q e$, where e is the elementary charge, and $Z_q = -1$ for electrons and $Z_q = 1$ for protons. The magnetic field of the system is described by the vector potential $\mathbf{A}(R, Z, \varphi, \tilde{t}) = (A_R = 0, A_Z, A_\varphi)$. The radial component A_R is set to zero, because of a gauge invariance. The electric field is given by the scalar potential $\Phi(R, Z, \varphi, \tilde{t})$. The time variable is notated by $\tilde{t}$.

The Hamiltonian GC equations are derived by the transformation of the canonical variables $(R, Z, \varphi, P_R, P_z, P_\varphi)$ of a gyrating particle to the canonical ones $(\vartheta_R, Z_c, \varphi_c, I_R, P_{zc}, P_{\varphi c})$ of the GC motion. Here (P_R, P_z, P_φ) are momenta canonically conjugated to the coordinates (R, Z, φ), and (ϑ_R, I_R) are the conjugated radial gyrophase and the action variables introduced for the fast gyrating motion of particle along the radial coordinate R. For the variables $(\vartheta_R, Z_c, \varphi_c, I_R, P_{zc}, P_{\varphi c})$ one obtains the six–dimensional (6-D) system of Hamiltonian equations.

In typical tokamak configurations the variable I_R can be treated as an adiabatic invariant. Then the Hamiltonian GC equations can be reduced to the 4-D system of equations, thus reducing the three–degrees of freedom of system to the two–degrees one.

Furthermore, we will omit subscript "c" in all variables and use the normalized variables

$$\begin{aligned} &x = R/R_0, && z = Z/R_0, \\ &p_z = P_Z/m_0\omega_0 R_0, && p_\varphi = P_\varphi/m_0\omega_0 R_0^2, \\ &t = \omega_0 \tilde{t}, \end{aligned} \tag{2.1}$$

where $\omega_0 = eB_0/m_0 c$ is a reference gyrofrequency, B_0 is the toroidal magnetic field strength at the torus center R_0, c is the speed of light in vacuum. We introduce also the reference energy $E_{ref} = m_0\omega_0^2 R_0^2$. The Hamiltonian equations for the canonical GC variables $(q_1, q_2, p_1, p_2) = (z, \varphi, p_z, p_\varphi)$ are

$$\frac{dq_i}{dt} = \frac{\partial H}{\partial p_i}, \qquad \frac{dp_i}{dt} = -\frac{\partial H}{\partial q_i}, \qquad (i = 1, 2). \tag{2.2}$$

with the Hamiltonian function given by

$$H = \varepsilon_0 \left[1 + \frac{2\omega_x I_x}{\varepsilon_0} + \frac{u_\varphi^2}{\varepsilon_0} \right]^{1/2} + Z_q \phi, \tag{2.3}$$

where $u_\varphi = (p_\varphi + Z_q \psi)/x_c$, $\varepsilon_0 = m_0 c^2/E_{ref} = (c/\omega_0 R_0)^2$ is a normalized energy of a particle at rest. The quantities,

$$\begin{aligned} &\psi \equiv \psi(x_c, z, \varphi, t) = -RA_\varphi/B_0 R_0^2, \\ &\phi \equiv \phi(x_c, z, \varphi, t) = e\Phi/E_{ref}, \end{aligned} \tag{2.4}$$

are the normalized toroidal component of the vector potential and the normalized scalar potential of the electric field. Here $I_x = \omega_0 I_R/E_{ref}$ is the normalized action variable. The radial component of the GC coordinate x_c, $(x_c = R_c/R_0)$ is a function of the canonical variables $(z, \varphi, p_z, p_\varphi)$ and determined by the balance equation of the centripetal force to the Lorentz force. When the typical toroidal fields it can be approximated as $x_c = \exp(-p_z/Z_q)$. The normalized radial gyrofrequency $\omega_x = \omega_R/\omega_0$ is then determined by $\omega_x = |Z_q| \exp(p_z/Z_q)$.

Since the runaway electrons (REs) are passing particles one can also reformulate Hamiltonian equations by introducing the toroidal angle φ as the independent, time-like variable and the corresponding canonical momentum p_φ as a new Hamiltonian $K = -p_\varphi$. The Hamiltonian equations for the canonical guiding–center variables $(q_1, q_2, p_1, p_2) =$

$(z, t, p_z, p_t = -H)$ have the form similar to (2.2) with the Hamiltonian function $K = K(z, t, p_z, p_t, \varphi)$

$$K = Z_q\psi(x, z, \varphi, t) - \sigma x_c u_\varphi, \tag{2.5}$$

where

$$\begin{aligned} u_\varphi &\equiv u_\varphi(x, z, \varphi, t, p_t) = \left[\varepsilon_0(\gamma_t^2 - 1) - 2\omega_x I_x\right]^{1/2}, \\ \gamma_t &= \frac{-p_t - Z_q\phi}{\varepsilon_0} \end{aligned} \tag{2.6}$$

is the relativistic factor. For the co-passing particles ($\sigma = +1$) the set of Hamiltonian equations (2.7) should be integrated along the positive direction of the toroidal angle φ, and vice versa for counter–passing particles ($\sigma = -1$).

The system of Hamiltonian equations can be written down as

$$\begin{aligned} \frac{dz}{d\varphi} &= \frac{\partial K}{\partial p_z} = \frac{x_c}{Z_q}\Big[- Z_q\frac{\partial\psi}{\partial x_c} + \frac{\sigma}{u_\varphi}\Big(\varepsilon_0(\gamma_t^2 - 1) - \omega_x I_x - x_c\gamma_t Z_q\frac{\partial\phi}{\partial x_c}\Big)\Big], \\ \frac{dp_z}{d\varphi} &= -\frac{\partial K}{\partial z} = -Z_q\left(\frac{\partial\psi}{\partial z} + \frac{\sigma\gamma_t x_c}{u_\varphi}\frac{\partial\phi}{\partial z}\right), \\ \frac{dt}{d\varphi} &= \frac{\partial K}{\partial p_t} = \frac{\sigma\gamma_t x_c}{u_\varphi}, \\ \frac{dp_t}{d\varphi} &= -\frac{\partial K}{\partial t} = -Z_q\left(\frac{\partial\psi}{\partial t} + \frac{\sigma\gamma_t x_c}{u_\varphi}\frac{\partial\phi}{\partial t}\right). \end{aligned} \tag{2.7}$$

The ratio $\lambda_I = I_x/T_K$ of the gyromotion energy, I_x, to the full kinetic energy of a particle, $T_k = \varepsilon_0(\gamma_t - 1)$, is considered as the initial parameter of motion. From the experimental measurements it follows that the parameter λ_I may reach a value of 0.1 (Finken *et al.* 1990; Jaspers 1995). Furthermore we will assume that $\lambda_I \leq 0.1$.

The system of equations (2.7) for the guiding–center motion can be presented in the form similar to the equations for magnetic field lines in the cylindrical coordinate system (R, Z, φ). Using the definitions,

$$B_R = B_\varphi\frac{\partial\psi}{\partial z}, \qquad\qquad B_Z = -\frac{B_0}{x}\frac{\partial\psi}{\partial x}, \tag{2.8}$$

where $B_\varphi = R_0B_0/R$ is the toroidal magnetic field, and the relations (2.1), one can reduce the system (2.7) to the one with real variables

$$\begin{aligned} \frac{dZ}{d\varphi} &= \frac{RB_Z^*}{B_\varphi} - \frac{\sigma R^2}{v_\varphi B_\varphi R_0}\frac{\partial\Phi}{\partial R}, & \frac{dR}{d\varphi} &= \frac{RB_R}{B_\varphi} + \frac{\sigma R^2}{v_\varphi B_\varphi R_0}\frac{\partial\Phi}{\partial Z}, \\ \frac{d\tilde{t}}{d\varphi} &= \frac{\sigma R}{v_\varphi}, & \frac{dH}{d\varphi} &= -Z_q\frac{\partial(RA_\varphi)}{\partial\tilde{t}} + Z_q\frac{\sigma R}{v_\varphi}\frac{\partial\Phi}{\partial t}, \end{aligned} \tag{2.9}$$

where $v_\varphi = u_\varphi R_0\omega_0/\gamma_t$ is the toroidal velocity. The quantity B_Z^* given by

$$B_Z^* = B_Z + \frac{\sigma B_\varphi}{Z_q}\left(u_\varphi + \frac{\omega_x I_x}{u_\varphi}\right). \tag{2.10}$$

can be called as the effective poloidal field. In the absence of the potential electric field

$\Phi \equiv 0$, we have

$$\frac{dZ}{d\varphi} = \frac{RB_Z^*}{B_\varphi}, \qquad \frac{dR}{d\varphi} = \frac{RB_R}{B_\varphi},$$
$$\frac{d\tilde{t}}{d\varphi} = \frac{\sigma R}{v_\varphi}, \qquad \frac{dH}{d\varphi} = -Z_q \frac{\partial (RA_\varphi)}{\partial \tilde{t}}. \tag{2.11}$$

3. Models of equilibrium magnetic field

In a cylindrical plasma the safety factor profile can be found by the density profile of the toroidal plasma current $j(\rho)$. The poloidal magnetic field B_θ is determined by according to the Ampère's law

$$B_\theta(R,Z) = \frac{\mu_o I(\rho)}{2\pi\rho} = \frac{\mu_o}{\rho}\int_0^r j(\rho')\rho' d\rho',$$

where $I(\rho)$ is the current flowing inside the magnetic surface of radius ρ. The safety factor $q(\rho)$ in the cylindrical geometry is defined as

$$q_{cyl}(\rho) = \frac{\rho B_0}{RB_\theta} = \frac{2\pi\rho^2 B_0}{\mu_o R_0 I(\rho)}. \tag{3.1}$$

The value of the safety factor at the plasma edge $\rho = a$ is determined by the total plasma current I_p,

$$q_a = q_{cyl}(a) = \frac{2\pi a^2 B_0}{\mu_o R_0 I_p}. \tag{3.2}$$

Consider the model plasma current given by the density

$$j(\rho) = \begin{cases} \dfrac{I_p(\nu+1)}{\pi a^2}\left(1-\rho^2/a^2\right)^\nu, & \text{for } \rho \le a, \\ 0, & \text{for } \rho > a, \end{cases} \tag{3.3}$$

where ν in the constant parameter. Then

$$I(\rho) = \begin{cases} I_p\left[1-\left(1-\rho^2/a^2\right)^{\nu+1}\right], & \text{for } \rho \le a, \\ I_p, & \text{for } \rho > a, \end{cases} \tag{3.4}$$

The safety factor $q_{cyl}(r)$ corresponding to this plasma current distribution is given by

$$q_{cyl}(\rho) = \begin{cases} q_a \dfrac{\rho^2/a^2}{1-(1-\rho^2/a^2)^{\nu+1}}, & \text{for } \rho \le a, \\ q_a\rho^2/a^2, & \text{for } \rho > a. \end{cases} \tag{3.5}$$

The value of the safety factor at the magnetic axis $q(0)$ is determined by q_a and ν: $q(0) = q_a/(\nu+1)$.

The toroidal corrections to the safety factor can be also found in the limit of large aspect ratio $R/r \gg 1$. The expansion of the safety factor in a series of powers $\varepsilon = \rho/R_p(\rho)$ is given by (see, (Abdullaev *et al.* 1999; Abdullaev 2006)),

$$q(\rho) = q_{cyl}(\rho)\frac{R_0^2}{R_p^2(\rho)}\left(1+\frac{1}{2}a_2\varepsilon^2+\frac{3}{8}a_4\varepsilon^4\right)+O(\varepsilon^8), \tag{3.6}$$

where $q_{cyl}(\rho)$ is the safety factor in the cylindrical geometry (3.1). The coefficients a_m

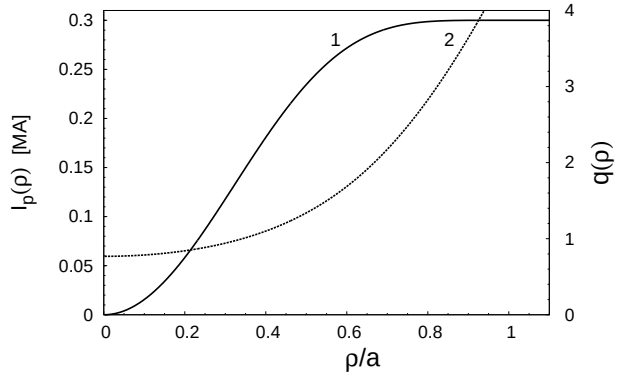

FIGURE 1. Radial profile of the plasma current $I_p(\rho)$ (3.4) (solid curves 1 on l.h.s. axis) and the safety factor profile $q(\rho)$ (3.6) (dashed curves 2 on r.h.s. axis). The plasma parameters are $I_p = 300$ kA, $B_0 = 2.4$ T, $R_0 = 1.75$ m, $a = 0.46$ m. The values of $q(0) = 0.8$.

are polynomial functions of the plasma parameter $\Lambda = \beta_{pol} + l_i/2 - 1$:

$$a_m = (-1)^m \sum_{k=0}^{m} (m - k + 1)\, \Lambda^k. \tag{3.7}$$

Here l_i is the plasma inductance. The plasma current profile $I_p(\rho)$ (3.4) and the safety factor profile $q(\rho)$ are plotted in Figure 1 for the full plasma current $I_p = 0.3$ MA and $q(0) = 0.8$.

4. An electron in an inductive electric field

In this section we recall the dynamics of electrons in the presence of the toroidal electric field induced by the plasma current decay during the plasmas disruption (Abdullaev 2015). Such an electric field can be introduced by the toroidal component of the inductive vector potential $A_\varphi^{(ind)}(\tilde{t})$ (Knoepfel & Spong 1979),

$$\begin{aligned} E_\varphi(R, Z, \tilde{t}) &= -\frac{\partial A_\varphi^{(ind)}(\tilde{t})}{\partial \tilde{t}}, \\ A_\varphi^{(ind)}(R, Z, \tilde{t}) &= \int^{\tilde{t}} \left[\frac{V(\tilde{t})}{2\pi R} - \frac{1}{R} \frac{\partial}{\partial \tilde{t}} \int_{r_R}^{b} R B_p(r, \tilde{t}) dr \right] d\tilde{t}, \end{aligned} \tag{4.1}$$

where $V(\tilde{t})$ is the loop voltage. The second term in the bracket of (4.1) describes the poloidal flux change due to rise or fall of the plasma current.

Then the poloidal flux ψ in the Hamiltonian function (2.3) is given by

$$\begin{aligned} &\psi = -\frac{RA_\varphi}{B_0 R_0^2} = \psi^{(0)}(x, z) + \psi^{(ind)}(x, z, t), \\ &A_\varphi = A_\varphi^{(0)}(R, Z) + A_\varphi^{(ind)}(R, Z, \tilde{t}), \\ &\psi^{(0)}(x, z) = -\frac{RA_\varphi}{B_0 R_0^2}, \qquad \psi^{(ind)}(x, z, t) = -\frac{RA_\varphi^{(ind)}(R, Z, t)}{B_0 R_0^2}. \end{aligned} \tag{4.2}$$

Here $A_\varphi^{(0)}(R, Z)$ is the toroidal component of the vector potential related to the equilibrium plasma. In normalized variables the inductive poloidal flux $\psi^{(ind)}(x, z, t)$ can be

presented as

$$\psi^{(ind)}(x,z,t) = -\frac{RA_\varphi^{(ind)}(R,Z,t)}{B_0R_0^2} = \int^t \mathcal{E}_\varphi(x,z,t')dt', \tag{4.3}$$

where $\mathcal{E}_\varphi(t)$ is the normalized toroidal electric field

$$\mathcal{E}_\varphi(x,z,t) = \frac{RE_\varphi(R,Z,\tilde{t})}{B_0R_0^2\omega_0} = \frac{V_\varphi(R,Z,t)}{2\pi B_0R_0^2\omega_0}. \tag{4.4}$$

Here $\tilde{t}$ is replaced by the normalized time $t = \omega_0\tilde{t}$. Then the change of the energy is given by

$$\frac{dH}{dt} = \frac{\partial H}{\partial t} = Z_q\frac{\partial h_c}{\partial p_\varphi}\frac{\partial \psi}{\partial t} = \frac{Z_qu_\varphi}{x_c\gamma_t}\mathcal{E}_\varphi(t). \tag{4.5}$$

The energy grows if $Z_qu_\varphi\mathcal{E}_\varphi(t) > 0$. Furthermore, we assume that the loop voltage V and thus $\mathcal{E}_\varphi(t)$ are constants in the poloidal section. Then the increment of particles energy in one poloidal turn is given by

$$\Delta H = \int_t^{t+T}\frac{dH}{dt}dt = Z_q\int_t^{t+T}\frac{d\varphi}{dt}\mathcal{E}_\varphi(t)dt \approx Z_q\mathcal{E}_\varphi(t)\Delta\varphi, \tag{4.6}$$

where $\Delta\varphi$ is the increment of the toroidal angle φ in one poloidal turn and T is the normalized transition time. Introducing the effective safety factor $q_{eff} = |\Delta\varphi|/2\pi$ (see Sec. 6.1) the energy increment ΔE in real variables can be written as

$$\Delta E = E_{ref}\Delta H = \sigma q_{eff}V_\varphi. \tag{4.7}$$

Now we estimate the outward drift velocity v_{dr} of orbits in a toroidal electric field. Suppose that the toroidal plasma has axisymmetry along the toroidal angle φ, i.e., $\psi = \psi(x,z,t)$ and $u_\varphi = u_\varphi(x,p_t)$. Then the toroidal momentum p_φ is constant of motion. According to (2.5) the drift surface at the time instant t is determined by the surface

$$K = -p_\varphi = f(x,z) = Z_q\psi(x,z,t) - \sigma x u_\varphi(x,p_t) = \text{const}, \tag{4.8}$$

where the poloidal flux $\psi(x,z,t)$ is given by (4.2). According to the latter and (4.6) in one poloidal turn the poloidal flux ψ and the energy $H = -p_t$ get increments $\Delta\psi = TZ_q\mathcal{E}_\varphi$ and ΔH, respectively. Since the increment $\Delta K = 0$ the drift surface shifts along the radial direction. Let Δx be a corresponding shift. From (4.8) one can obtain the expression for Δx:

$$\Delta x = \frac{Z_q}{\left(Z_q\dfrac{\partial\psi}{\partial x} - \dfrac{\sigma}{u_\varphi}\left[\varepsilon_0(\gamma_t^2-1) - \omega_xI_x\right]\right)}\left(x\frac{2\pi q_{eff}\gamma_t}{u_\varphi} - T\right)\mathcal{E}_\varphi. \tag{4.9}$$

From (4.9) we obtain the formula for the outward drift velocity

$$v_{dr} = \omega_0\frac{\Delta R}{T} = \frac{E_\varphi}{B_z^*}\left(\frac{R_0}{R} - \frac{T_{av}}{\widetilde{T}}\right), \tag{4.10}$$

where B_z^* is the effective poloidal field given by (2.10), $\Delta R = R_0\Delta x$ is the radial shift of an orbit, $\widetilde{T} = \omega_0^{-1}T$ is the actual transit time. The quantity $T_{av} = 2\pi q_{eff}R_0/v_\varphi$ is an average transition time. The formula (4.10) quite well reproduces the numerically calculated outward drift velocities.

In particularly case $T_{av} = \widetilde{T}$, $\sigma = 1$ and for low–energy electrons when $B_z^* \approx B_z$ the

formula (4.10) can be reduced to the one obtained by (Guan *et al.* 2010; Qin *et al.* 2011) for the circular GC orbits,

$$v_{dr} = -\frac{E_\varphi \left(R - R_0\right)}{RB_z}. \tag{4.11}$$

One should note that the expression (4.10) describes not only the outward drift velocity of electron orbits but also the inward drift (the Ware pinch) velocity of trapped electrons. More detailed discussion of the drifts of electron orbits in the toroidal electric field can be found in Abdullaev (2015).

5. Models of magnetic perturbations

5.1. *Model of MHD modes*

The magnetic perturbations due to the MHD modes can described by the vector potential $A_\varphi^{(1)}(R, Z, \varphi, t)$. We present as sum

$$A_\varphi^{(1)}(R, Z,\varphi, t) = -\frac{R_0^2}{R}\sum_{mn} m^{-1} B_{mn} U_{mn}(\rho)\cos\left(m\vartheta - n\varphi + \Omega_{mn}t + \chi_{mn}\right), \tag{5.1}$$

where Ω_{mn} is the frequency of the $(m, n)-$th mode and χ_{mn} is its phase. The quantities B_{mn} are the amplitudes of MHD modes and the functions $U_{mn}(\rho)$ describe the radial profiles of the modes. In (5.1) ϑ is the poloidal angle in which the field lines are linear functions of the toroidal angle φ: $\vartheta = \varphi/q(\rho) + \vartheta_0$.

The radial profiles of MHD modes $U_{mn}(\rho)$ in realistic tokamak plasmas is less known. As will be shown in Sec. 7.2 the structure of magnetic field lines is less sensitive to the form of the radial profile of MHD modes. Only requirement is that the amplitudes $U_{mn}(\rho)$ should vanish at the magnetic axis $\rho = 0$, i.e., $U_{mn}(0) = 0$. We choose the following model for the radial dependence of the functions U_{mn} that satisfies this condition:

$$U_{mn} = \left[1 - \exp\left(-\frac{\rho^2}{2a^2\Delta}\right)\right], \tag{5.2}$$

where Δ is a constant parameter.

The perturbation poloidal flux $\psi_\varphi^{(1)} = -RA_\varphi^{(1)}/B_0R_0^2$ is given by

$$\psi_\varphi^{(1)}(R, Z, \varphi, t) = \sum_{mn} m^{-1} b_{mn} U_{mn}(\rho)\cos\left(m\vartheta - n\varphi + \omega_{mn}t + \chi_{mn}\right). \tag{5.3}$$

One can introduce a dimensionless perturbation parameter ϵ_{MHD} as

$$\epsilon_{MHD} = \max\left|\frac{B_{mn}}{B_0}\right| = \max|b_{mn}|, \tag{5.4}$$

where $b_{mn} = B_{mn}/B_0$ are the normalized amplitudes of MHD modes. For example, for $\epsilon_{MHD} = 7.0 \times 10^{-5}$ and B_0 =2.5 T we have $B_{mn} = 1.75 \times 10^{-4}$ T= 1.75 G.

5.2. *Model of the DED magnetic perturbations*

Below we briefly describe the magnetic perturbations created by the DED coils of the TEXTOR (see, (Finken *et al.* 2005) and Appendix A in (Abdullaev 2014)). It consists of 12 helical conductors installed on the inboard side of the TEXTOR vessel. The sketch of the DED coil configuration in the poloidal section is shown in Fig. 7. The corresponding perturbation magnetic field can be approximated by the toroidal component of the vector

n	$\tilde{\phi}_n$	ι_n
1	$3\pi/16$	$\sin(\pi/4)/[4\sin(\pi/16)]$
2	$3\pi/8$	$1/[2\sin(\pi/8)]$
4	$5\pi/4$	$\sqrt{2}$

TABLE 1. Coefficients ϕ_h and ι_n for the different n.

potential,

$$A_\varphi^{(DED)}(R,Z,\varphi) = -\frac{B_c R_0^2}{R}\sum_m m^{-1} a_{mn}(r)\cos\left(m\theta + n\varphi + \phi_n - \Omega t\right). \tag{5.5}$$

The coefficient a_{mn} determined by the geometrical configuration of coils is given by

$$\begin{aligned} a_{mn}(r) &= \iota_n\sqrt{\frac{R_0}{R}}\frac{r_c g_{mn} R}{R_0^2}\left(\frac{r}{r_c}\right)^{|m|}, \\ g_{mn} &= (-1)^m C_m \frac{\sin[(m+nm_0/4)\theta_c]}{(m+nm_0/4)\pi}, \\ C_m &= \frac{\sin[(m+nm_0/4)\Delta\theta/2]}{(m+nm_0/4)\Delta\theta/2}. \end{aligned} \tag{5.6}$$

It describes the poloidal mode spectrum at the given toroidal mode n. In Eq. (5.5) the quantity $B_c = \mu_0 m_0 I_{ded}/\pi r_c$ is the characteristic magnitude of the DED magnetic field, I_{ded} is the DED current, the constant m_0 determines the central poloidal mode number $nm_0/4$, r_c is the minor radius of the DED coils, and Ω is the rotation frequency of the perturbation field.

In (5.5) (r,θ,φ) are the quasi-toroidal coordinates related to the cylindrical coordinates R, Z as $r = \sqrt{(R-R_o)^2 + Z^2}$ and $\theta = \arctan(Z/[R-R_0])$. In a toroidal system the angle θ does not coincide with the poloidal ϑ. The relation between ϑ and the geometrical angle θ, i.e., $\vartheta = \vartheta(\theta;\rho)$ depends on the equilibrium plasma. In a toroidal system the relation between ϑ and θ can be presented by a series in powers of the inverse aspect ratio $\varepsilon = \rho/R_0$ (see Ch. 2 in (Abdullaev 2014) for more details). In the first order we have

$$\vartheta = \theta + a_1\varepsilon\sin\theta + \cdots, \tag{5.7}$$

where $a_1 = -(2+\Lambda)$. [For $\beta_{pol} = 0, l_i = 1.2$ one has $a_1 = -1.6$.]

The toroidal mode number n takes the value $n = 4$ for the so–called 12/4 operational mode, $n = 2$ for the 6/2 mode, and $n = 1$ for the 3/1 mode, respectively. The dependencies of the coefficients g_{mn} on m in these operational modes are plotted in Fig. 2 The radial decay of the radial component of the perturbation field $B_r = -r^{-1}\partial A_\varphi/\partial\theta$ in these modes is proportional to $(r/r_c)^{nm_0/4}$. The phases ϕ_n and the factor ι_n in Eq. (5.5) are determined by the coil configuration. For the particular configuration they given by

$$\phi_n = \frac{m_0 n}{4}(\pi - \theta_0) - \tilde{\phi}_n + \frac{\pi}{2}, \tag{5.8}$$

where θ_0 is a poloidal angle of the first coil at the section $\varphi = 0$. The coefficients $\tilde{\phi}_n$ and ι_n for the different values of$n$ are given in Table 1.

Similar to (5.3) and (5.4)) one can also introduce the perturbation poloidal flux $\psi^{(1)}$

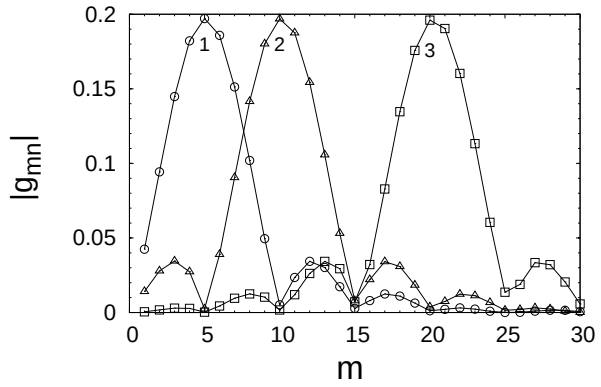

FIGURE 2. Dependence of the coefficients g_{mn} on the mode number m in the three different operational modes: 3/1 mode (curve 1), 6/2 mode (curve 2), and 12/4 mode (curve 3).

and the dimension perturbation parameter ϵ_{MHD},

$$\epsilon_{DED} = \frac{B_c}{B_0} = \frac{\mu_o m_0 I_{ded}}{\pi r_c B_0}. \tag{5.9}$$

The parameters r_c, θ_c, θ_0, $\Delta\theta$, and m_0 are determined by the geometry of coil configuration, and take fixed values, $r_c = 0.5325$ m, $\theta_c = 35.49°$, $\theta_0 = 169.35°$, $\Delta\theta = 17.745°$, and $m_0 \approx 20$.

This model of the DED fields well describes the qualitative and quantitative features of heat deposition patterns observed in the TEXTOR–DED experiments (Jakubowski *et al.* 2006; Finken *et al.* 2005).

6. Dynamics of REs in the toroidal plasmas

6.1. *The equations of motion in action–angle variables*

Below we present the equations of GC motion in the action–angle variables (Sec. 5.2 in (Abdullaev 2014)). Such a formulation allows one to better understand the effect of magnetic perturbations on electrons and magnetic field lines.

In the absence of non-axisymmetric perturbations, i.e., $\epsilon = 0$, the Hamiltonian functions (2.3), (2.5) do not explicitly depend on the toroidal angle φ, i.e., $H = H_0(z, p_z, p_\varphi)$, $[K = K(z, p_z, E)]$. In this case field lines and particle guiding center trajectories lie on the toroidal surfaces (or drift surfaces) defined by $H(z, p_z, E)$ =const and p_φ =const, respectively. To describe such a motion one can introduce the action–angle variables $(\vartheta_z, \vartheta_\varphi, J, I_\varphi)$ associated with the canonical variables $(z, \varphi, p_z, p_\varphi)$:

$$J = \frac{1}{2\pi} \oint\limits_{C_z} p_z(z; h_c, p_\varphi) dz, \qquad I_\varphi = p_\varphi,$$
$$\vartheta = \frac{\partial S}{\partial J}, \qquad \vartheta_\varphi = \frac{\partial S}{\partial I_\varphi}, \tag{6.1}$$

determined by the generating function,

$$S = S(z, \varphi, J, I_\varphi) = \varphi I_\varphi + \int^z p_z(z'; h_c, I_\varphi) dz'. \tag{6.2}$$

The integrals in (6.1) and (6.2) ares taken along the closed contour C_z formed by the

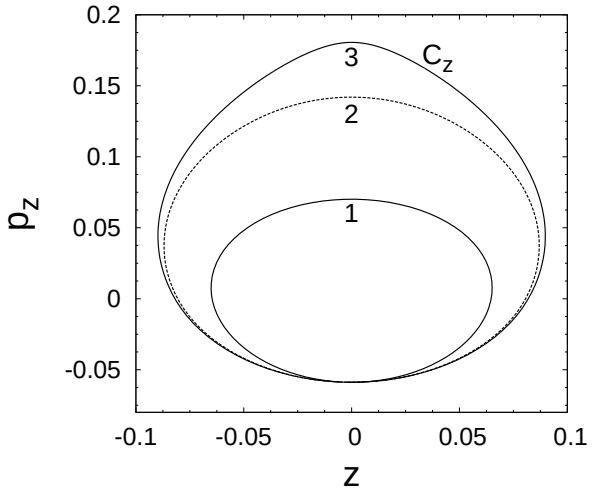

FIGURE 3. Closed contours C_z of orbits in the (z, p_z) plane. Curve 1–3 correspond to RE with different energies: $1 - E = 10$ keV, $2 - E = 40$ MeV, and $3 - E = 42.5$ MeV The plasma parameters: $B_t = 2.5$ T, $I_p = 150$ kA.

projection of the drift orbit in the $(z, p_z)-$ plane as shown in Fig. 3.

In the action–angle variables the Hamiltonian H depends on the action variables (J, I_φ), $H = H_0(J, I_\varphi)$. The unperturbed motion is characterized by the poloidal, $\omega(J, I_\varphi) = \partial H_0/\partial J$, and the toroidal, $\omega_\varphi(J, I_\varphi) = \partial H_0/\partial I_\varphi$, frequencies of the conditionally-periodic motion on the drift surface, known as transit oscillations (or *bounce oscillations*). The particle trajectories $(z(t), p_z(t), \varphi(t), p_\varphi)$ are $2\pi-$periodic functions of the angle variables $\vartheta_z, \vartheta_\varphi$:

$$\begin{aligned} &z(\vartheta_z, J, I_\varphi) = z(\vartheta_z + 2\pi, J, I_\varphi), \\ &p_z(\vartheta_z, J, I_\varphi) = p_z(\vartheta_z + 2\pi, J, I_\varphi), \\ &\varphi(\vartheta_z, \vartheta_\varphi, J, I_\varphi) = \varphi(\vartheta_z + 2\pi, \vartheta_\varphi + 2\pi, J, I_\varphi). \end{aligned} \tag{6.3}$$

Particularly, the relation between the toroidal angle φ and the angle variables is given by

$$\varphi = \vartheta_\varphi + G(\vartheta_z, J, I_\varphi), \tag{6.4}$$

where $G(\vartheta_z, J, I_\varphi)$ is the $2\pi-$periodic function of ϑ_z. The angle variables $\vartheta_z, \vartheta_\varphi$ are the linear functions of time

$$\begin{aligned} \vartheta_z &= \omega_z(J, I_\varphi)t + \vartheta_{z0}, \\ \vartheta_\varphi &= \omega_\varphi(J, I_\varphi)t + \vartheta_{\varphi 0}. \end{aligned} \tag{6.5}$$

For passing particles one introduce the quantity similar to the safety factor $q(\psi)$. It is called the effective safety factor q_{eff} and is defined as the ratio of the increment of the toroidal angle φ per one poloidal turn, i.e., $q_{eff} = \Delta\varphi/2\pi$. From (6.5) it follows that $q_{eff} = \omega_\varphi(J, I_\varphi)/\omega_z(J, I_\varphi)$ and it depends on the particle energy.

One should note the dependence of the effective safety factor q_{eff} on the particle energy. For low–energy electrons q_{eff} coincides with the safety factor $q(\rho)$ of the equilibrium magnetic field. With increasing the electron energy the effective safety factor strongly deviates from $q(\rho)$. Particularly, with approaching RE energy E to the critical energy

E_{cr} of the separatrix the transit time T as well as q_{eff} diverge as

$$T =\propto \ln \frac{B}{|E-E_{cr}|}, \qquad q_{eff} \propto \ln \frac{C}{|E-E_{cr}|}, \tag{6.6}$$

where B and C are constant coefficients.

6.2. *Effect of magnetic perturbations on GC orbits*

In the presence of magnetic perturbations, given, for instance, by (5.1) or (5.5), the action variables are not constants of motion. Their time–evolution are described by the perturbed Hamiltonian equations

$$\begin{aligned} \frac{d\vartheta_z}{dt} &= \frac{\partial H}{\partial J}, & \frac{dJ}{dt} &= -\frac{\partial H}{\partial \vartheta_z}, \\ \frac{d\vartheta_\varphi}{dt} &= \frac{\partial H}{\partial I_\varphi}, & \frac{dI_\varphi}{dt} &= -\frac{\partial H}{\partial \vartheta_\varphi}, \end{aligned} \tag{6.7}$$

with the Hamiltonian $H(\vartheta_z, \vartheta_\varphi, J, I_\varphi, t)$ depending on the all canonical variables and time. In tokamaks the magnetic perturbations are small in compared to the main equilibrium field. In this case it is convenient to present the Hamiltonian H is a sum

$$H = H_0(J, I_\varphi) + \epsilon H_1(\vartheta_z, \vartheta_\varphi, J, I_\varphi, t), \tag{6.8}$$

where

$$H_1(\vartheta_z, \vartheta_\varphi, J, I_\varphi, t) \approx \frac{Z_q}{\gamma_t} \frac{u_\varphi \psi^{(1)}}{x_c}, \tag{6.9}$$

is the perturbation Hamiltonian, $u_\varphi = (p_\varphi + Z_q\psi_0)/x_c$, ϵ stands for the dimensionless perturbation parameter ϵ_{MHD} (5.4) [or ϵ_{DED} (5.9)]. Since the perturbation are periodic in poloidal and toroidal angles and in time it can be presented by a Fourier series

$$H_1(\vartheta_z, \vartheta_\varphi, J, I_\varphi, t) = \sum_{mn} H_{mn}(J, I_\varphi) \exp\left[i\left(m\vartheta_z - n\vartheta_\varphi + \Omega_{mn}t\right)\right]. \tag{6.10}$$

First we consider the MHD magnetic perturbations described in Sec. 5.1. Using the expansion (5.1) for the perturbation poloidal flux $\psi^{(1)}$, the Fourier components $H_{mn}(J, I_\varphi)$ can reduced to the integrals of type

$$H_{mn}(J, I_\varphi) = (2\pi)^{-2} \iint_0^{2\pi} d\vartheta_z d\vartheta_\varphi \sum_{m'n'} c_{m'n'} e^{i\left(m'\vartheta - m\vartheta_z - n'\varphi + n\vartheta_\varphi\right)}, \tag{6.11}$$

where the angles ϑ and φ associated with magnetic field lines are considered as functions of ϑ_z and ϑ_φ. Similar to (6.4) the relation between ϑ and ϑ_z can be also presented as

$$\vartheta = \vartheta_z + F(\vartheta_z, J, p_\varphi), \tag{6.12}$$

where $F(\vartheta_z, J, p_\varphi)$ is $2\pi-$periodic function of ϑ_z. The functions $F(\vartheta_z, J, p_\varphi)$ and $G(\vartheta_z, J, p_\varphi)$ depend on electron's energy E and vanish at $E \to 0$. The coefficients c_{mn} are proportional to the MHD mode amplitudes a_{mn}, i.e., $c_{mn} = (Z_q u_\varphi/x_c)a_{mn}$. They are not only functions of (J, I_φ) but also slowly varying functions of ϑ_z and ϑ_φ.

For low energy electrons with energies less several MeVs the GC orbits are close to the magnetic field lines, and one can approximate $\vartheta_z \approx \vartheta$ and $\vartheta_\varphi \approx \varphi$. Then from (6.11) it follows that $H_{mn}(J, I_\varphi) \approx c_{mn}(J, I_\varphi)$, i.e., the perturbation spectra of low–energy electrons are close the spectra of magnetic perturbations.

With increasing electron's energy the relation and (6.12) between ϑ and ϑ_z become

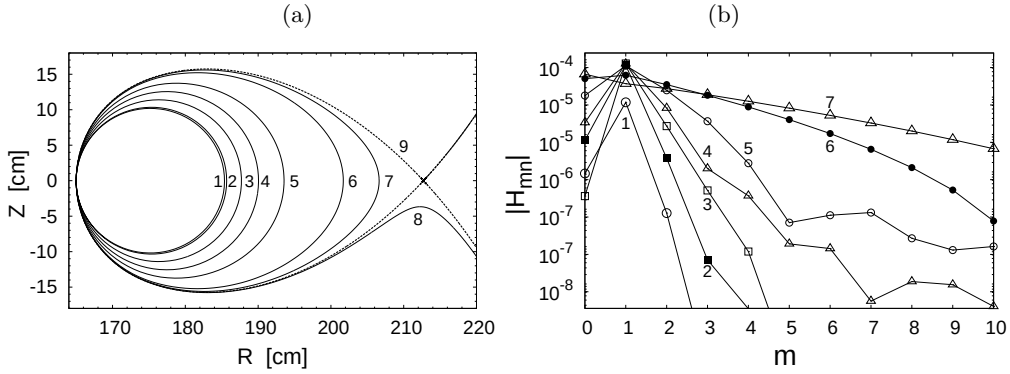

FIGURE 4. (a) RE orbits with different energies E and (b) spectrum of perturbations H_{mn} corresponding to these orbits. Curves 1–8 correspond to RE energies 10 keV, 1 MeV, 10 MeV, 20 MeV, 30 MeV, 40 MeV, 42 MeV, and 42.8 MeV, respectively. Curve 9 corresponds to the separatrix with the critical energy $E_{cr} = 42.646$ MeV. The plasma current $I_p = 150$ kA, the toroidal field $B_0 = 2.5$ T. The toroidal mode number $n = 1$.

strongly nonlinear, while the relation between toroidal angle φ and ϑ_φ given by (6.4) is almost linear. Thus the perturbation spectra of high–energy electrons $H_{mn}(J, I_\varphi)$ may have much higher m-th harmonics than the spectra of magnetic perturbations a_{mn} with the same toroidal mode number n.

Figures 4 (a) and (b) illustrates the dependence of the RE orbits and the perturbation spectrum H_{mn} on the electron energy E. It is assumed that the magnetic perturbation (5.1) contains only the single mode ($m = 1, n = 1$). One can see that with increasing electron energy its orbit evolves from the circular form to the oval one shown by curves 1 to 7. When the energy exceed a certain critical energy E_{cr} the electron becomes unconfined and strikes wall as shown by curve 8 in Fig. 4 (a). The separatrix (curve 9) corresponds to the critical energy E_{cr}.

For the low energy electrons with $E < 10$ MeV the spectrum H_{mn} contains the predominant $m = 1$ mode. With increasing the energy the amplitudes H_{mn} of higher m also grow and the poloidal spectrum H_{mn} in poloidal mode m becomes wider as shown in Fig. 4 (b). For the spectrum H_{mn} one can obtain the following asymptotical formula for the orbits close to the separatrix (see Sec. 3.4 in (Abdullaev 2014))

$$H_{mn} \propto \frac{1}{T} \exp\left(-\frac{mC}{T}\right), \tag{6.13}$$

where C is a finite constant, and the transit time T diverges as (6.6).

In the case of the DED magnetic perturbation described in Sec. 5.2 one obtains the expressions for H_{mn} similar to (6.11) in which the variable ϑ should be replaced by the geometrical angle θ. The latter should be considered as a function of ϑ_z. Unlike the previous case the perturbation spectrum H_{mn} does not coincide $c_{mn} = (Z_q u_\varphi / x_c) a_{mn}$, where a_{mn} is given by (5.6), for the both, for low–energy electrons and as for high–energy electrons. It is because that the geometrical angle θ does not coincide with the poloidal angle ϑ of magnetic field lines. For low–energy electrons the spectrum of perturbation H_{mn} will be close to magnetic perturbations the features of which has been studied in detail in Refs. (Finken *et al.* 2005; Abdullaev 2014). With increasing the energy of particles the contribution of higher (m, n) mode harmonics of H_{mn} will grow.

Figure 5 shows the spectrum of perturbation H_{mn} in the case of the DED magnetic perturbations with the toroidal modes $n = 1$ (a) and $n = 2$ (b) for the electron orbits in

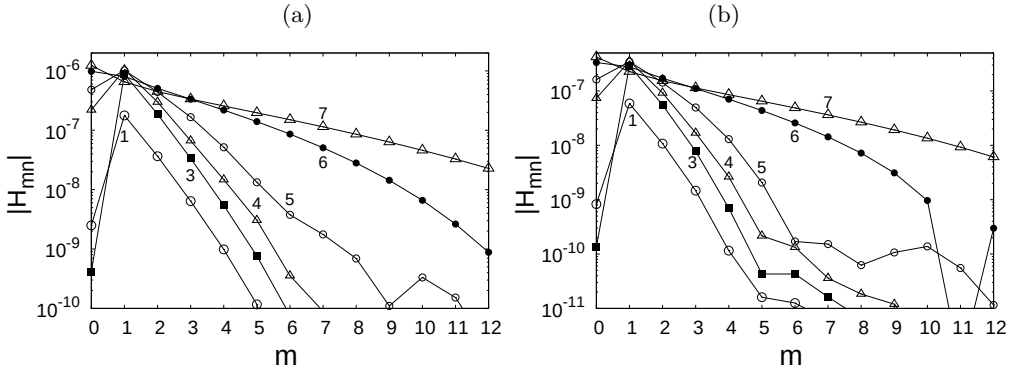

FIGURE 5. Spectrum of perturbations H_{mn} in the presence of the magnetic perturbations of the DED field. Numbering of curves corresponding to the orbits in Fig. 4 (a). The plasma parameters are also the same. The toroidal mode numbers $n = 1$ (a) and $n = 2$ (b).

Fig. 4 (a). As in the case of a single mode magnetic perturbation shown Fig. 4 (b) the mode $m = 1$ has a highest amplitude since according to (5.6) it has a weak radial decay $H_{mn} \propto r$. However, with increasing the electron energy the amplitudes H_{mn} of higher harmonics $m > 1$ grow and near the separatrix has the asymptotics (6.13) and (6.6).

6.3. *Resonance interactions of REs with magnetic perturbations*

From (6.10) it follows that a particle's orbit is strongly affected near the resonant drift surfaces determined by the condition,

$$m\omega_z(J, I_\varphi) - n\omega_\varphi(J, I_\varphi) + \Omega_{mn} = 0. \tag{6.14}$$

The particles near this resonant drift surface can be trapped into the island. Such particle islands are shown in Fig. 6 (a) and (b).

The resonant condition (6.14) for the relativistic electrons in the presence of low–frequency magnetic perturbations can be rewritten in a more simple form. Indeed, since the frequency $\Omega_{mn} \sim 10^5$ s^{-1} and $\omega_z \approx c/(2\pi q R_0) \sim 10^7$ s^{-1} one can neglect the ratio $\Omega_{mn}/\omega_z \sim 10^{-2} \ll 1$. Then we have

$$m - nq_{eff}(J, I_\varphi) = 0, \tag{6.15}$$

which similar to the condition for resonant magnetic surfaces, but the safety factor q of magnetic surfaces is replaced by the effective safety factor $q_{eff}(J, I_\varphi)$ of drift surfaces.

Let J_{mn}, I_φ be the value of J and I_φ (or energy E) corresponding to the isolated resonant surface (m, n). The width of the island $\Delta J, \Delta I_\varphi$ along the variables J, I_φ is determined by the magnitude of $H_{mn}(J, I_\varphi)$ at the resonant drift surface and given by (see Sec. 8.1 in (Abdullaev 2014))

$$\Delta J = mW_{mn}, \qquad \Delta I_\varphi = nW_{mn}, \tag{6.16}$$

where

$$\begin{aligned} W_{mn} &= 4\sqrt{\epsilon |V_{mn}/\kappa_{mn}|}, \\ V_{mn} &= H_{mn}\left(mJ_{mn}, J_\varphi - nJ_{mn}\right), \\ \kappa_{mn} &= \left(m\frac{\partial\widetilde{\Omega}}{\partial J} - n\frac{\partial\widetilde{\Omega}}{\partial I_\varphi}\right), \\ \widetilde{\Omega} &= m\omega_z(J, I_\varphi) - n\omega_\varphi(J, I_\varphi). \end{aligned} \tag{6.17}$$

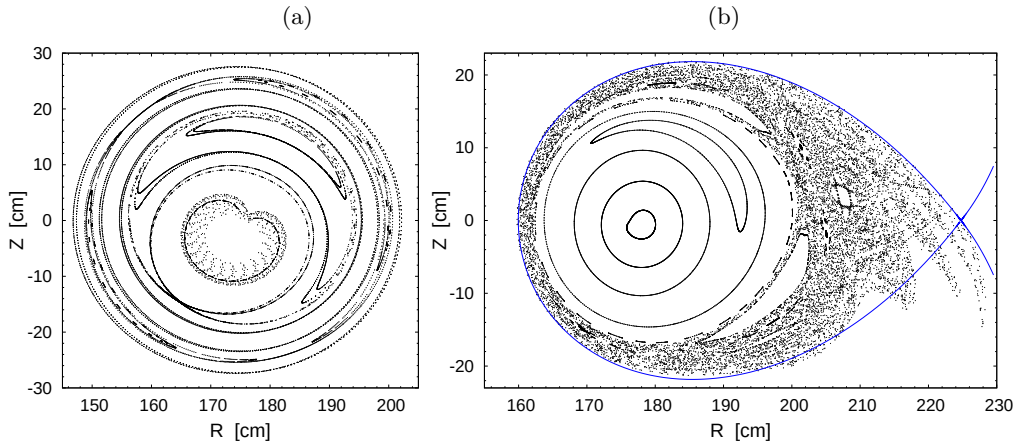

FIGURE 6. Poincaré sections of RE orbits in the (R, Z)-plane: Red dots correspond to RE orbits with energies $E = 1$ MeV (a) and $E = 30$ MeV (b). The perturbation parameter $\epsilon = 4 \times 10^{-5}$, the plasma currents $I_p = 230$ kA (a) and $I_p = 150$ kA (b), the toroidal field $B_0 = 2.5$ T.

The quantity $J_\varphi = nJ + mI_\varphi$ is the integral of motion.

If there are several closely located islands in a system, they may overlap at the certain level of magnetic perturbation which leads to the chaotic motion of particles. According to (6.13) and (6.6) the spectrum of perturbations H_{mn} for particles of energy close to the critical one E_{cr} becomes much wider while the distances $\delta J = |J_{m+1} - J_m|$ between resonances gets smaller which certainly leads to overlapping of these chains of islands. The particles in the stochastic zone formed due to this process quickly loose the confinement and hit the wall.

Examples of such stochastic zones are shown in Figs. 6 (b) and 7. Particularly, Figs. 7 (a)-(c) show how the structure of orbits evolves with the increase of particle energy. Particles of 10 MeV energy interact with the $(m = 1, n = 1)$ magnetic perturbations forming a number of high–order isolated resonances shown in Fig. 7 (a). For particles with higher energy these resonances overlap forming a stochastic zone open to the wall (7 (b)-(d)).

7. Model of a stochastic magnetic field

Below we describe the model of magnetic field in the disruptive stage of a tokamak plasma. This model will be used to study the stochastization of magnetic field lines due to interaction of low mode number nonlinear MHD modes and to estimate a heat and particle transport in the corresponding stochastic magnetic field.

7.1. *Field line equations*

Field lines are governed Hamiltonian field line equations

$$\frac{d\vartheta}{d\varphi} = \frac{\partial\psi}{\partial\psi_t}, \qquad \frac{d\psi_t}{d\varphi} = -\frac{\partial\psi}{\partial\vartheta}, \tag{7.1}$$

with the poloidal flux $\psi \equiv \psi(\psi_t, \vartheta, \varphi)$ is being the Hamiltonian function and the poloidal angle ϑ and the toroidal flux ψ_t are being as the canonical coordinate and momenta. The toroidal angle φ is an independent time–like variable. The poloidal flux ψ can be presented as a sum of the unperturbed flux $\psi_0(\psi_t)$ of the equilibrium plasma and the perturbation part $\psi_1(\psi_t, \vartheta, \varphi)$ arising from the magnetic perturbations caused by the

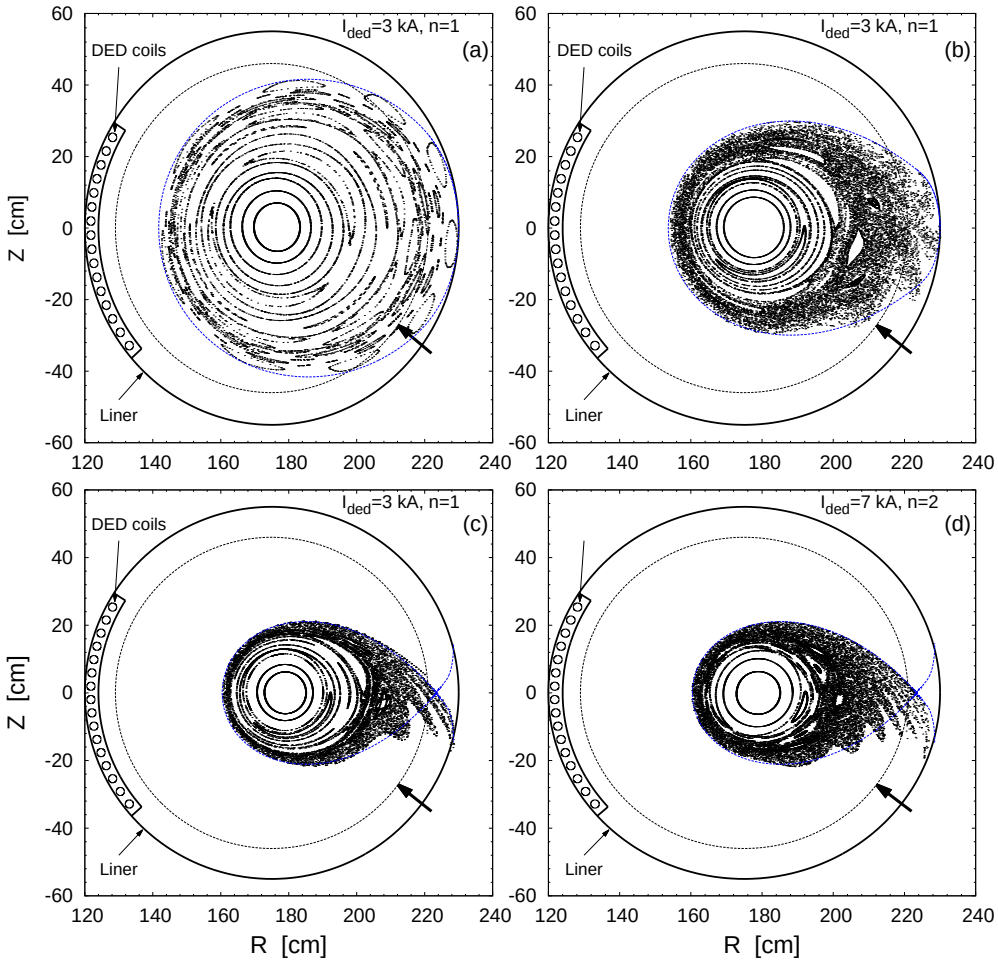

FIGURE 7. Poincaré sections of RE orbits in the (R, Z)-plane of the RE orbits in the presence of the magnetic perturbations of the TEXTOR-DED. Electron energy: (a) $E = 10$ MeV; (b) $E = 20$ MeV; (c) $E = 30$ MeV; for the $n = 1$ mode with the perturbation current $I_{ded} = 3$ kA.; (d) $E = 30$ MeV for the $n = 2$ mode with $I_{ded} = 7$ kA; The plasma current $I_p = 150$ kA, the toroidal field $B_t = 2.4$ T.

MHD modes,

$$\psi(\psi_t, \vartheta, \varphi) = \psi_0(\psi_t) + \psi_1(\psi_t, \vartheta, \varphi), \tag{7.2}$$
$$\psi_0(\psi_t) = \int \frac{d\psi_t}{q(\psi_t)},$$
$$\psi_1(\psi_t, \vartheta, \varphi) = \sum_{m,n} \epsilon_{mn} U_{mn}(\psi_t) \cos\left(m\vartheta - n\varphi + \chi_{mn}\right).$$

The dimensionless parameters ϵ_{mn} stand for the relative magnitudes of magnetic perturbations: $\epsilon_{mn} \sim B_{mn}/B_0$, where B_{mn} is the amplitude of the MHD modes. The quantities χ_{mn} describe the phases of magnetic perturbations.

Furthermore we use the toroidal flux ψ_t by normalizing to its value $\Psi_a \approx a^2/2R_0^2$ at the plasma boundary $\rho = a$. Then the toroidal flux $\psi_t = \rho^2/a^2$ takes values in the

interval $[0,1]$, where ρ is the minor radius and a is the plasma radius. For this setting the relation between ϵ_{mn} and the amplitudes of the MHD modes ϵ_{MHD} b_{mn} (5.2), (5.4) is given by $\epsilon_{mn} = \epsilon_{MHD} b_{mn}/\Psi_a$.

Furthermore we use the model (3.5) for the safety factor which in the flux variable ψ_t is reduced to

$$q(\psi_t) = q_a \frac{\psi_t}{1-(1-\psi_t)^{q_a/q_0}}, \tag{7.3}$$

where $q_0 = q(0)$ is the value of safety factor at the magnetic axis $\psi_t = 0$, $q_a = q(a)$ is the value of safety factor at the plasma boundary $\psi_t = 1, (r = a)$, q_b is the parameter. This model for the safety factor fairly well describe the experiment in the TEXTOR tokamak. The safety factor profiles for the different values of q_0 for the full plasma current $I_p = 300$ kA are given in Fig. 1 by curves 2.

7.2. *Model of MHD modes*

Now we turn to models for the amplitudes $U_{mn}(\psi_t)$ of the low mode number MHD modes which causes a plasma disruption. The main requirement is that the magnetic perturbations $U_{mn}(\psi_t)$ should go to zero at the magnetic axis $\psi_t = 0$ (or $\rho = 0$), i.e., $U_{mn}(\psi_t = 0) = 0$. As we will see below the structure of magnetic field lines in the presence of magnetic perturbations is mainly determined by the amplitudes of modes $U_{mn}(\psi_t)$ at the resonant magnetic surfaces $\psi_t = \psi_{mn}$, it is less sensitive to the radial profiles of $U_{mn}(\psi_t)$, i.e., on the form of dependence of $U_{mn}(\psi_t)$ on ψ_t. Below we consider two models for the amplitudes $U_{mn}(\psi_t)$ satisfying the similar condition at the magnetic axis but having different radial profiles.

The first simple model is given by

$$U_{mn}(\psi_t) = \frac{1}{m}\left(1 - e^{-\psi_t/\Delta}\right), \tag{7.4}$$

which is determined by only one parameter Δ. This radial profile corresponds to the MHD mode profiles given by Eq. (5.2).

The several realistic models for the MHD modes have been proposed in literature (see, e.g., (Igochine *et al.* 2006) and references therein). Below we use the model given in Ref. (Constantinescu *et al.* 2008) (Eq. (9)) which has been reconstructed from ECE measurements in the ASDEX tokamak. We rewrite it in the form

$$U_{mn}(\psi_t) = \frac{1}{m}\begin{cases} \dfrac{1}{1-\beta}\left[1-\beta\left(\bar{\psi}_t\right)^{1/2}\right]\left(\bar{\psi}_t\right)^{m/2}, \\ \qquad \text{for } \bar{\psi}_t \le 1, \\ \left[1-\delta+\delta\left(\bar{\psi}_t\right)^{1/2}\right]\left(\bar{\psi}_t\right)^{-(m+1)/2}, \\ \qquad \text{for } \bar{\psi}_t > 1, \end{cases} \tag{7.5}$$

where $\bar{\psi}_t = \psi_t/\psi_{mn}$. In this form the profiles $mU_{mn}(\rho)$ takes a unit value at the resonant magnetic surface $\psi_t = \psi_{mn}$. The formula (7.5) depends on the parameters β and δ unlike the original one which depends on the three parameters. Then the amplitude of modes is given by the dimensionless perturbation parameters ϵ_{mn}.

Figure 8 (a) and (b) show the profiles of $mU_{mn}(\rho)$ for the models (7.4) and (7.5), respectively, at the different values of Δ. The structure of field lines are mainly determined by the values of mode amplitudes U_{mn} at the resonant surfaces $\psi_t = \psi_{mn}$ rather then their radial profiles. It is illustrated in Fig. 9 by plotting Poincaré sections of field lines for the two different radial profiles of $U_{mn}(\psi_t)$ given by (7.4) and (7.5) (see Fig. 8 (a), (b)).

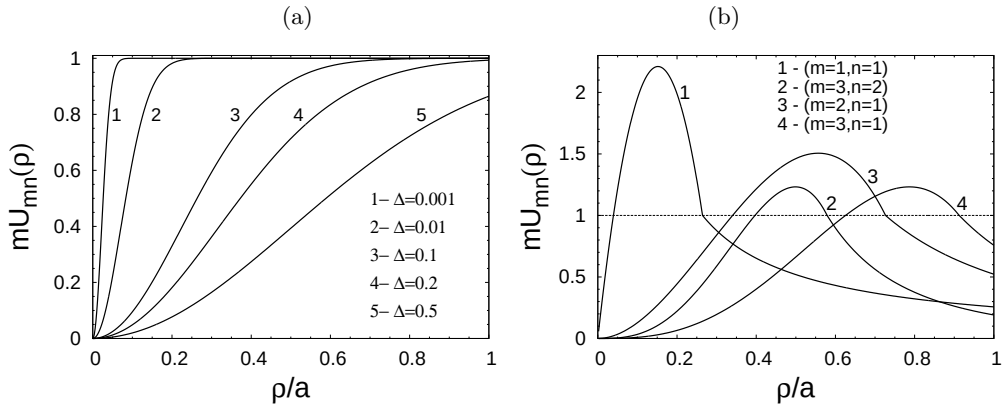

FIGURE 8. Radial profiles of perturbation modes mU_{mn}: (a) corresponds to the profile (7.4); (b) corresponds to (7.5) with the parameters: $\alpha = 0.04$, β =0.87, $\gamma = 0.005$, $\delta = 0.9615$. The radial positions $\rho_{mn} = a\sqrt{\psi_{mn}}$ correspond to the resonant surfaces $q(\psi_{mn}) = m/n$ for the safety factor (7.3) with $q_0 = 0.9$ and $q_a = 3.6$.

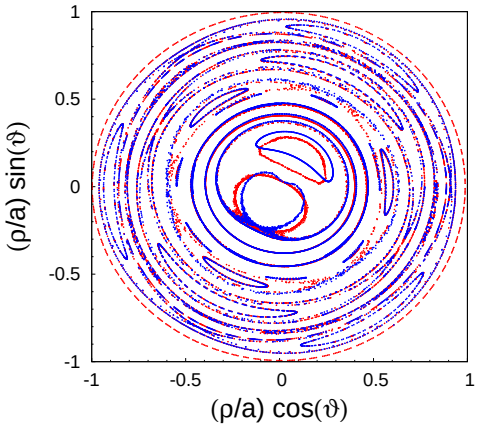

FIGURE 9. Poincaré sections for the radial profiles of the MHD modes: blue dots corresponds (7.4) (see also Fig. 8 (a)); red dots corresponds to (7.5) (see also Fig. 8 (b)). The parameters: $\Delta = 0.001$, $\epsilon_{mn} = 2 \times 10^{-3}$ $(n = 1, 2,\ m = 1 - 4)$, $q_0 = 0.9$ and $q_a = 3.6$.

The structure of majority magnetic islands is less sensitive to the radial profiles of MHD modes. It is related with the fact in the pendulum approximation the form of the nonlinear resonance created by the MHD modes is mainly determined by the values of its amplitude $U_{mn}(\psi_t)$ at the resonant surfaces $\psi_t = \psi_{mn}$ (see, for example, Sec. 8.1 in Abdullaev (2014)). Only the structure of the mode $n = 1, m = 1$ depends on the radial profile of $U_{mn}(\psi_t)$, especially at the region close to the magnetic axis. But the outer region of the island is less dependent on the profile of $U_{mn}(\psi_t)$.

7.3. *Possible structures of a stochastic magnetic field during plasma disruptions*

Using the above model of magnetic field one can study possible structures of magnetic field during plasma disruptions. It is believed that the plasma disruption is caused by the large–scale magnetic stochasticity created by the interactions of nonlinearly excited low-order (m, n) MHD modes: $(1/1, 2/1, 3/2, 4/3, \dots)$.

First we consider structures of magnetic field during plasma disruptions corresponding to the plasma with a monotonic radial profile of the safety factor $q(\psi_t)$ (7.3) shown in

Fig. 1. Figures 10 (a)–(d) shows Poincaré sections of field lines in the presence several low–order MHD modes and with the different amplitudes ϵ_{11} of the $(m = 1, n = 1)$ mode. The interaction of these modes leads to the strong chaotic behavior of field lines. At the small amplitudes of the $(m = 1, n = 1)$ mode, shown in Fig. 10 (a), the chaotic field lines are formed only in outer region. The central plasma region is separated from the chaotic region by the *magnetic transport barrier* formed between the magnetic surface $q = 1$ and $q = 5/3$. The stochastic layer formed near the separatrix of the magnetic island $(m = 1, n = 1)$ is negligible small. With increasing ϵ_{11} the magnetic transport barrier moves toward toward the plasma center and the width of the stochastic layer of the the magnetic island $(m = 1, n = 1)$ grows as shown in Fig. 10 (b). Starting from the certain level of ϵ_{11} the transport barrier disappears and the stochastic layer of the island $(m = 1, n = 1)$ joins the outer chaotic zone (Fig. 10 (c)). The further increase of ϵ_{11} shrinks the stability region of of the island $(m = 1, n = 1)$ (Fig. 10 (d)).

Now we consider the plasmas with a reversed magnetic shear, i.e., with a *non-monotonic radial profile* of the safety factor $q(\psi_t)$. The formation of the stochastic zone in this case is different from the case with the monotonic safety factor profile. The magnetic transport barrier is formed near the so–called *shearless magnetic surface* where $q(\psi_t)$ takes minimal value. Such a magnetic surface is relatively stable even to large magnetic perturbations. The latter does not shrink the shearless magnetic surface but only deforms it †.

To illustrate this we consider the plasma with the following safety factor profile

$$q(\rho) = \frac{q_m}{1 - b(\rho^2 - \rho_m^2)^2}, \tag{7.6}$$

shown in Fig. 11 (a). Here q_m is a minimal value of $q(\rho)$, ρ_m is the shearless magnetic surface, b is constant. The parameters ρ_m and b can be expressed through the values of the safety factor at the magnetic axis $q(0)$, the plasma edge $q(a)$, and q_m.

Poincaré sections of magnetic field lines are plotted in Fig. 11 (b)-(d) for the different amplitudes of magnetic perturbations ϵ_{mn} with the radial profiles (7.4). As seen the magnetic transport barrier (a red curve) located near the shearless magnetic surface $\rho = \rho_m$ does not shrink with the increase of perturbations.

In the cases shown in Figs. 10 (a), (b) and Fig. 11 (b)-(d) the central region of plasma is confined and the radial transport of particles there is much small than in the chaotic region. The acceleration of electrons in this confined region by the toroidal electric field may lead to the formation of RE beams.

7.4. *Collisional transport in a stochastic magnetic field*

The transport of heat and charged particles in a stochastic magnetic field has been studied since early 1970s in the numerous works (see Abdullaev (2013), Sec. 10.4 in Abdullaev (2014) and Sec. 9.8 in White (2014) for references). In general this problem has a three–dimensional nature because of the system's asymmetry along poloidal and toroidal directions in the presence of magnetic perturbations ((Runov *et al.* 2001; Feng *et al.* 2008; Frerichs *et al.* 2012) and references therein). However, the problem can be simplified when we are interested only in the radial transport averaged over poloidal and toroidal angles. In this case the heat transport along the radial coordinate can be characterized by only the radial heat conductivity coefficient χ_r which in turn is determined by the radial diffusion coefficient D_r of electrons.

Below we calculate the diffusion coefficient D_r in a stochastic magnetic field during the plasma disruption. For this we use the collisional test particle transport model described

† The detailed description such systems known as *non-twist systems* and references can be found in monographs by Abdullaev (2006, 2014).

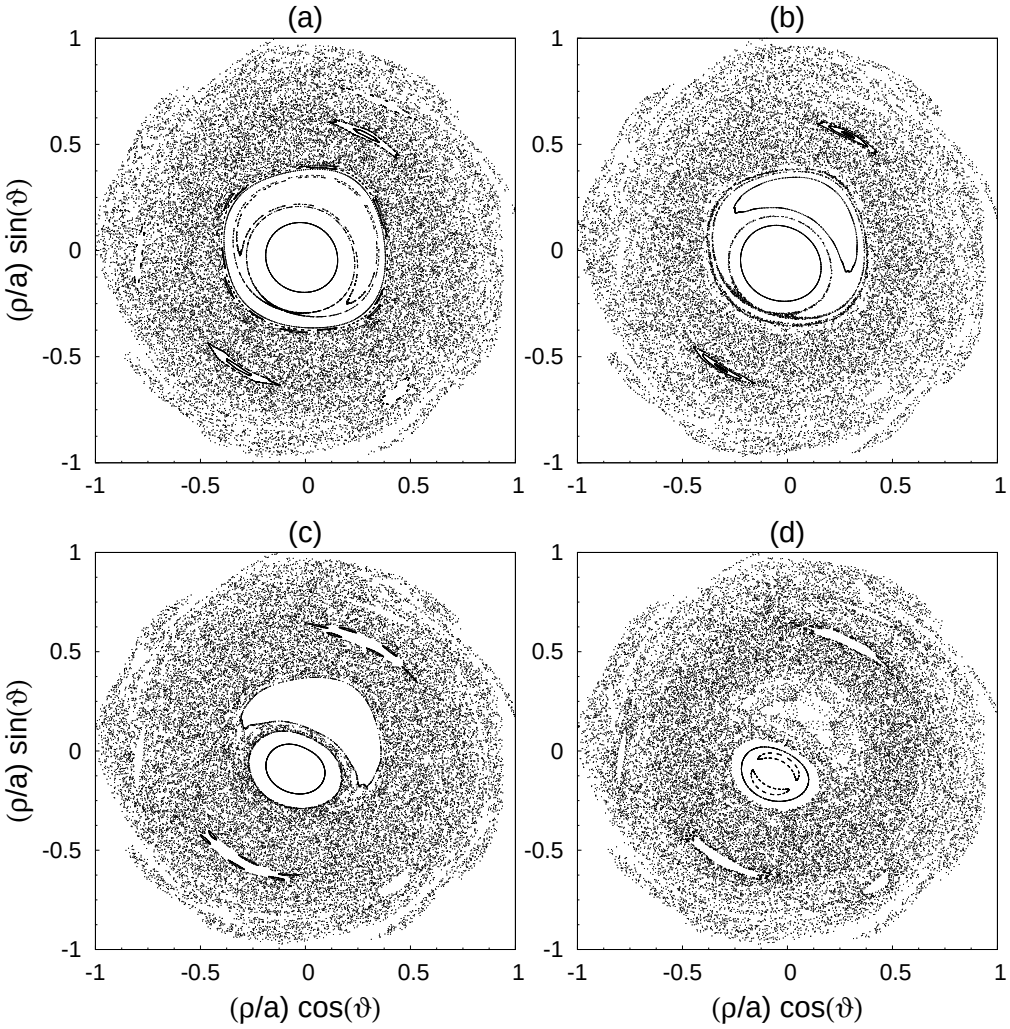

FIGURE 10. Poincaré sections of field lines in a pre–disruption plasma caused by a several MHD modes with the different amplitudes of the $(m = 1, n = 1)$ mode: (a) $\epsilon_{11} = 10^{-3}$; (b) $\epsilon_{11} = 2 \times 10^{-3}$; (c) $\epsilon_{11} = 4 \times 10^{-3}$; (d) $\epsilon_{11} = 8 \times 10^{-3}$. The amplitudes of all other modes are $\epsilon_{mn} = 4 \times 10^{-3}$ $(n = 1 - 3,\ m = 1 - 11)$. The safety factor at the magnetic axis is $q(0) = 0.8$ and at the plasma edge $q_a = 4.7$.

in (Abdullaev 2013, 2014) (see also (Rax & White 1992)). In this model a collisional particle motion in the presence of magnetic perturbations is considered as a random walk process along field lines and random jumps across magnetic surfaces.

The numerical procedure of this process is carried out in a following way: a particle moves freely along the field line with a step l after which it collides with other particle with the probability p, $(0 < p < 1)$. After the collision it changes the direction of motion to the opposite one being simultaneously displaced to the distance $\delta\rho$ across a field line. The probability p is determined by the mean free path λ_{mfp}: $p = l/(l + \lambda_{mfp})$, while the displacement $\delta\rho$ is determined by the perpendicular diffusion coefficient $\chi_\perp$: $\delta\rho = \sqrt{2\chi_\perp/pv_\parallel}$, where $v_\parallel$ is a parallel velocity of a particle. The mean free path depends of the plasma temperature T_e and electrons $\lambda_{mfp} = 8.5 \times 10^{21} T_e/n_e$ m, where the electron temperature T_e [in keV] and the density n_e [in m^{-3}]. One should that the temperature and

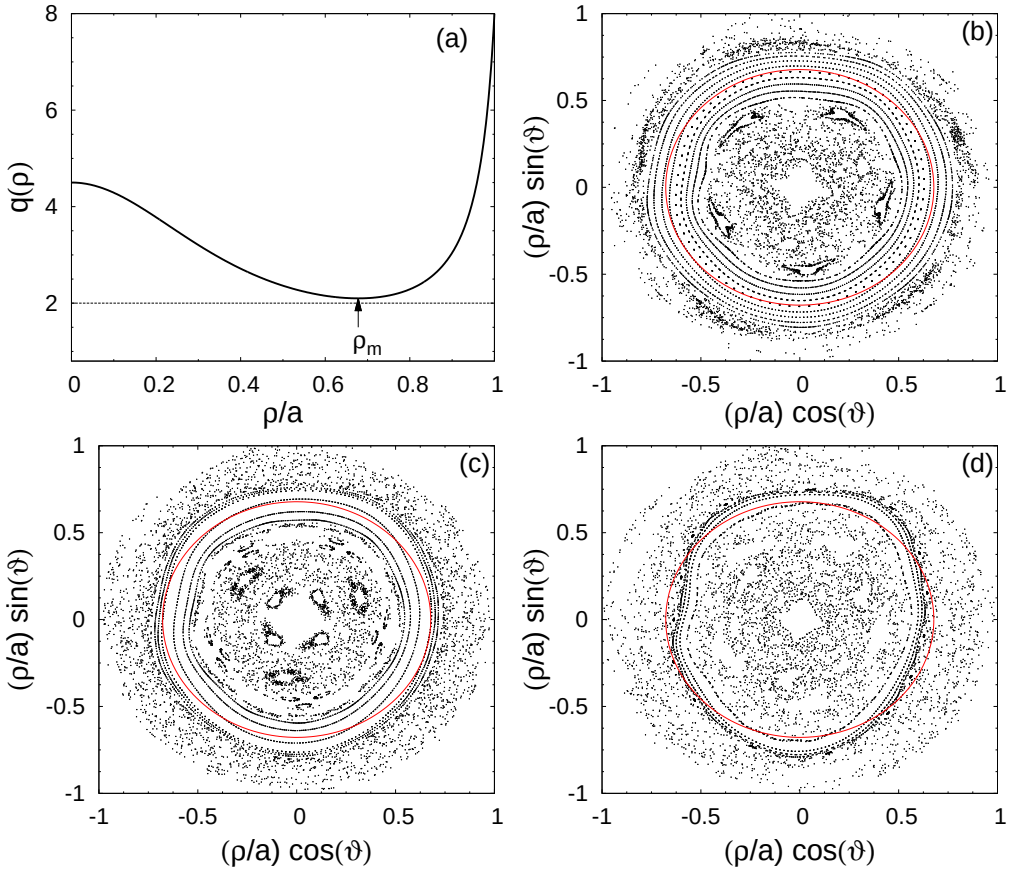

FIGURE 11. The same as in Fig. 10 but for the plasma with the reverse magnetic shear. (a) the safety factor profile $q(\rho)$; The amplitudes of all MHD modes are equal: (b) $\epsilon_{mn} = 10^{-3}$; (c) $\epsilon_{mn} = 5 \times 10^{-3}$; (d) $\epsilon_{mn} = 10^{-2}$; The safety factor at the magnetic axis is $q(0) = 4.5$, the minimal value $q_m = 2.1$, and at the plasma edge $q_a = 8.0$. The parameter Δ in (7.4) is taken equal to 0.5. Red curve corresponds to the unperturbed shearless magnetic surface $\rho = \rho_m$.

the density are local functions of the radial coordinate ρ: $T_e = T_e(\rho)$ and $n_e = n_e(\rho)$. The parallel velocity $v_\parallel$ can be taken equal to the electron thermal velocity $v_{T_e} = \sqrt{kT_e/m_e} = 1.33 \times 10^7\ T_e^{1/2}$ m/s, where k is the Boltzmann's constant.

The calculations are performed by integrating the field line equations (7.1) using the forward and the backward mapping procedures described in (Abdullaev 2013, 2006, 2014). The local diffusion coefficients D_r are found by fitting the dependence of the second moment $\langle(\Delta\rho)^2\rangle$ on time t by a linear function $2D_r t$ at the initial growth range of t. Figure 12 shows an example of the dependence of the local diffusion coefficient D_r of electrons on the local temperature T_e at the magnetic surface $\rho = 0.71a$ in a stochastic magnetic field shown in Fig. 10 (b).

As was shown in (Abdullaev 2013) the collisional diffusion coefficient D_r can be quite well described by the empirical formula

$$\chi_r(\rho, T_e) = \frac{v_\parallel D_{FL}(\rho)}{1 + L_c/\lambda_{mfp}}, \tag{7.7}$$

determined only by a few plasma parameters: the mean free path λ_{mfp}, the thermal

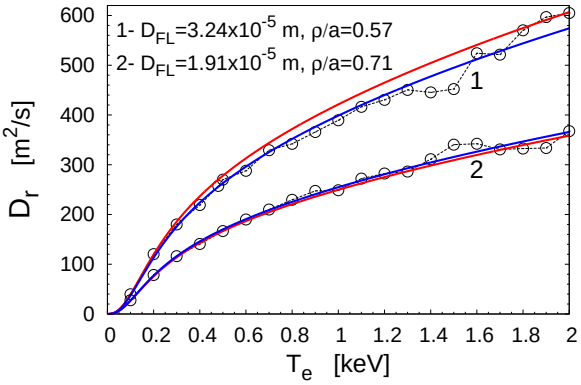

FIGURE 12. Dependence of the local radial diffusion coefficients D_r on the electron temperature T_e at the magnetic surfaces $\rho = 0.5a$ (curves 1) and $\rho = 0.71a$ (curves 2). The plasma density $n = 2 \times 10^{19}$ m^{-3}. The perturbation field parameters are the same as in Fig. 6 of the main text. Symbols "$\circ$" correspond to the numerical calculated D_r, red curves correspond to the empirical formula (7.7) for D_r, and blue curves correspond to the formula $D_r = \alpha\sqrt{T}/(1 + \beta/T^2)$ with the fitted coefficients α and β.

T_i [keV]	D_p [m^2/s]	$\tau_p = a^2/2D_p$ [s]
0.005	0.0986057	1.072
0.050	0.386249	2.739×10^{-1}
0.100	1.01251	1.045×10^{-1}
0.500	6.46228	1.637×10^{-2}
1.000	9.51915	1.111×10^{-2}
2.000	13.1030	8.074×10^{-3}
4.000	17.8366	5.932×10^{-3}
5.000	23.7424	4.456×10^{-3}
10.00	27.0265	3.915×10^{-3}

TABLE 2. Ambipolar diffusion coefficients D_p of particles and the diffusion times $\tau_p = a^2/2D_p$ from the stochastic zone at the different effective plasma temperatures. The plasma radius $a = 0.46$ m.

velocity v_{T_e}, the radial diffusion coefficient of field lines, D_{FL}, and the characteristic length L_c. The latter is an empirical parameter which has an order of the connection length $\pi q R_0$. As seen from Fig. 12 the empirical formula (red curve) well describes the temperature dependence of D_r.

The particle transport in a stochastic magnetic field can be also treated in a similar way. However, because of the ambipolarity of a particle transport instead of the thermal velocities of electrons v_{T_e} and ions $v_{T_i} = \sqrt{kT_i/m_i}$ in the test particle simulations one should use the sound speed $c_s = \sqrt{k(T_e + \gamma_i T_i)/m_i}$ where T_i is the ion temperature, m_i is the ion mass, and γ_i is the adiabatic index. This condition comes from the fact that the loss rates of electrons and ions are equal.

In Table 2 we have listed the values of the ambipolar diffusion coefficients D_p and the characteristic diffusion times $\tau_p = a^2/2D_p$ of particles from the stochastic zone at the different plasma temperatures $T_e = T_i$.

REFERENCES

Abdullaev, S. S. 2006 *Construction of Mappings for Hamiltonian Systems and Their Applications*. Heidelberg: Springer.

Abdullaev, S. S. 2013 On collisional diffusion in a stochastic magnetic field. *Phys. Plasmas* **20**, 082507.

Abdullaev, S. S. 2014 *Magnetic Stochasticity in Magnetically Confined Fusion Plasmas*. Cham–Heidelberg: Springer-Verlag.

Abdullaev, S. S. 2015 Drifts of electron orbits induced by toroidal electric field in tokamaks. *Phys. Plasmas* **22**, 030702.

Abdullaev, S. S. & Finken, K. H. 2002 Hamiltonian guiding center equations in a toroidal system. *Phys. Plasmas* **9**, 4193–4204.

Abdullaev, S. S., Finken, K. H. & Spatschek, K. H. 1999 Asymptotical and mapping methods in study of ergodic divertor magnetic field in a toroidal system. *Phys. Plasmas* **6**, 153–174.

Abdullaev, S. S., Wingen, A. & Spatschek, K. H. 2006 Mapping of drift surfaces in toroidal systems with chaotic magnetic fields. *Phys. Plasmas* **13** (4), 042509.

Constantinescu, D., Dumbrajs, O., Igochine, V. & Weyssow, B. 2008 On the accuracy of some mapping techniques used to study the magnetic field dynamics in tokamaks. *Nucl. Fusion* **48**, 024017.

Feng, Y., Kobayashi, M., Morisaki, T., Masuzaki, S., Miyazawa, J., Peterson, B. J., Morita, S., Shoji, M., Ida, K., Yamada, I., Narihara, K., Ashikawa, N., Yamada, H., Ohyabu, N., Komori, A., Morojima, O., Sardei, F., Reiter, D. & LHD Experimental Group 2008 Fluid features of the stochastic layer transport in LHD. *Nucl. Fusion* **48**, 024012.

Finken, K. H., Abdullaev, S. S., Jakubowski, M., Lehnen, M., Nicolai, A. & Spatschek, K. H. 2005 *The structure of magnetic field in the TEXTOR-DED*, *Energy Technology*, vol. 45. Jülich, Germany: Forschungszentrum Jülich.

Finken, K. H., Watkins, J. G., Rüsbuldt, D., Corbett, W. J., Dippel, K. H., Goebel, D. M. & Moyer, R. A. 1990 Observation of sychrotron radiation from tokamak runaway electrons in TEXTOR. *Nucl. Fusion* **30**, 859.

Frerichs, H., Clever, M., Feng, Y., Lehnen, M., Reiter, D. & Schmitz, O. 2012 Numerical analysis of particle recycling in the TEXTOR helical divertor. *Nucl. Fusion* **52** (3), 023001 (9pp).

Guan, X., Qin, H. & Fisch, N.J. 2010 Phase-space dynamics of runaway electrons in tokamaks. *Phys. Plasmas* **17** (9), 092502.

Igochine, V., Dumbrajs, O., Constantinescu, D., Zohm, H., Zvejnieks, G. & ASDEX Upgrade Team 2006 Stochastic sawtooth reconnection in ASDEX upgrade. *Nucl. Fusion* **46** (7), 741–751.

Jakubowski, M. W., Schmitz, O., Abdullaev, S. S., Brezinsek, S., Finken, K. H., Krämer-Flecken, A., Lehnen, M., Samm, U., Spatschek, K. H., Unterberg, B., Wolf, R. C. & the TEXTOR team 2006 Change of the magnetic-field topology by an ergodic divertor and the effect on the plasma structure and transport. *Phys. Rev. Lett.* **96**, 035004.

Jaspers, R. J. E. 1995 Relativistic runaway electrons in tokamak plasmas. PhD thesis, Eidenhoven University of Technology, The Netherlands.

Knoepfel, H. & Spong, D. A. 1979 Runaway electrons in toroidal discharges. *Nucl. Fusion* **19** (6), 785–829.

Qin, H., Guan, X. & Fisch, N. J. 2011 Neoclassical drift of circulating orbits due to toroidal electric fieldin tokamaks. *Tech. Rep.* PPPL-4639. Princeton Plasma Physics Laboratory, Princeton.

Rax, J. M. & White, R. B. 1992 Effective diffusion and nonlocal heat transport in a stochastic magnetic field. *Phys. Rev. Lett.* **68**, 1523–1526.

Runov, A. M., Reiter, D., Kasilov, S. V., Heyn, M. F. & Kernbicher, W. 2001 Monte Carlo study of heat conductivity in stochastic boundaries: Application to the TEXTOR ergodic divertor. *Phys. Plasmas* **8**, 916–930.

White, R. B. 2014 *The Theory of Toroidally Confined Plasmas*, 3rd edn. London: Imperial College Press.

Wingen, A., Abdullaev, S. S., Finken, K. H. & Spatschek, K. H. 2006 Influence of stochastic fields on relativistic electrons. *Nucl. Fusion* **46**, 941–952.